


# Ultra-low temperature synthesis of Ge-based optical materials and devices on Si using $\text{GeH}_3\text{Cl}^\dagger$

 Author and affiliation details can be edited in the panel that appears to the right when you click on the author list.


Aixin Zhang<sup>a</sup>, Matthew A. Mircovich<sup>b</sup>, Dhruve A. Ringwala<sup>a</sup>, Christian D. Poweleit<sup>b</sup>, Manuel A. Roldan<sup>c</sup>, José Menéndez<sup>b</sup> and John Kouvetakis, 0000-0003-4200-4950<sup>b,\*</sup>

<sup>a</sup>School of Molecular Sciences, Arizona State University, Tempe, AZ 85287-1604, USA

<sup>b</sup>Department of Physics, Arizona State University, Tempe, AZ 85287-1504, USA, [john.kouvetakis@asu.edu](mailto:john.kouvetakis@asu.edu)

<sup>c</sup>Eyring Materials Center, Arizona State University, Tempe, AZ 85287, USA

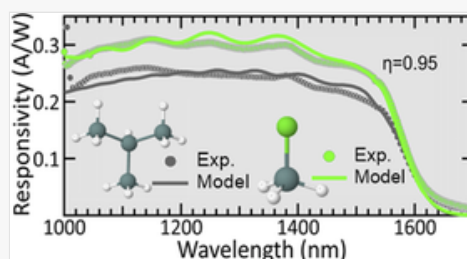
## Funding Information

 We have combined the funding information you gave us on submission with the information in your acknowledgements. This will help ensure the funding information is as complete as possible and matches funders listed in the Crossref Funder Registry.

Please check that the funder names and award numbers are correct. For more information on acknowledging funders, visit our website: <http://www.rsc.org/journals-books-databases/journal-authors-reviewers/author-responsibilities/#funding>.

Funder Name :	National Science Foundation
Funder's main country of origin :	
Funder ID :	10.13039/1000000001
Award/grant Number :	DMR-2119583

## Table of Contents Entry



CMOS-compatible  $\text{GeH}_3\text{Cl}$  is used to develop GeSn semiconductors and Ge/Si photodiodes. Responsivities of the latter display near ideal 0.95 collection efficiency (green) a ~~clear~~ performance improvement to devices made by other methods such as  $\text{Ge}_4\text{H}_{10}$  (black).

## Abstract

We describe an alternative strategy to the fabrication of Ge–Sn based materials on Si by using chlorogermane ( $\text{GeH}_3\text{Cl}$ ) instead of the specialty Ge hydrides ( $\text{Ge}_2\text{H}_6$ ,  $\text{Ge}_3\text{H}_8$ ,  $\text{Ge}_4\text{H}_{10}$ ) currently employed as ultra-low temperature sources of Ge. This simpler and potentially more practical chlorinated derivative is obtained in high yields and in research-grade purity by direct reactions of commercial  $\text{GeH}_4$  and  $\text{SnCl}_4$  and exhibits favorable physical and chemical properties that make it an effective source of Ge for a wide range of chemical vapor deposition (CVD) processing conditions. As a proof-of concept, we have employed  $\text{GeH}_3\text{Cl}$  to demonstrate deposition of pure Ge and GeSn heterostructures on large-area Si wafers, at conditions compatible with current specialty methods for next generation

technologies but with higher deposition efficiency, ensuring an optimal use of the Ge feedstock. In the case of pure Ge,  $\text{GeH}_3\text{Cl}$  has enabled growth of thick and uniform Ge layers with flat surfaces and relaxed microstructures at 330–360 °C, exhibiting lower residual doping than obtained by alternate Ge hydride methods.  $\text{GeH}_3\text{Cl}$  allows for *in situ* doping with the same facility as the Ge hydrides, and this has enabled the design and fabrication of homo-structure pin photodetectors exhibiting low dark current densities and closer to ideal optical collection efficiencies when compared to devices produced by other Ge-on-Si approaches. In the case of GeSn, the high reactivity of  $\text{GeH}_3\text{Cl}$  toward Sn hydrides has enabled the formation of mono-crystalline alloy layers at ultra-low temperatures between 200–300 °C and conditions akin to molecular beam epitaxy (MBE). Combined, these results suggest an intriguing potential for this new CVD process in the device-application space. The deployment of  $\text{GeH}_3\text{Cl}$  as a highly reactive low-temperature Ge-source could not only improve on the current wasteful methods that use  $\text{GeH}_4$ , but also eliminate the need for the higher-cost polygermanes.

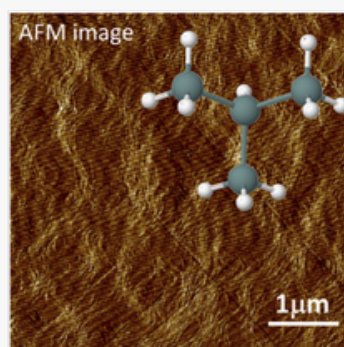
## 1. Introduction

In recent years there has been increasing interest in depositing crystalline Ge on Si at temperatures below 400 °C, driven by the dual desire to achieve full compatibility with complementary metal–oxide semiconductor (CMOS) processing and to develop suitable growth protocols for GeSn alloys. Conventional chemical-vapor deposition (CVD) precursors such as  $\text{GeH}_4$  are not ideally suited for this purpose. For pure Ge growth on Si using  $\text{GeH}_4$ , the films must be deposited at temperatures well above 400 °C to achieve optimal structural quality. For GeSn growth,  $\text{GeH}_4$  must be supplied in a hundredfold excess relative to the Sn sources to achieve the targeted compositions.<sup>1</sup> In addition to the Ge-source issues, the 400 °C constraint for the growth temperature also creates difficulties for device fabrication based on *in situ* doping protocols, since standard precursor gases such as  $\text{PH}_3$  and  $\text{AsH}_3$  require higher temperatures for optimal dopant activation.

The doping problem can be solved with new precursors introduced in recent years.<sup>2–7</sup> These precursors are compatible with low-temperature growth and have high levels of activation even without post-growth annealing. For some of the new compounds, including  $(\text{GeH}_3)_3\text{P}$ ,  $(\text{GeH}_3)_3\text{As}$ , and  $(\text{GeH}_3)_3\text{Sb}$ , the facile substitutional incorporation into the Ge-lattice can be rationalized as resulting from the preexistence of three dopant-host bonds in the precursor molecule.

Regarding the Ge-source, several approaches have been proposed to overcome the limitations of CVD based on  $\text{GeH}_4$ . A drastic solution was demonstrated by Park *et al.*, who deposited  $\alpha$ -Ge at 300 °C and obtained single-crystal Ge films by metal-induced crystallization at 360 °C.<sup>8</sup> Plasma-enhanced CVD (PECVD) methods have also been used.<sup>9–11</sup> The above target threshold of 400 °C has been reached by Alharthi *et al.*<sup>11</sup> albeit with a relatively broad FWHM of 0.26° for the (004) X-ray reflection. An alternative approach to low-temperature Ge on Si is the use of polygermanes of the form  $\text{Ge}_n\text{H}_{2n+2}$  with  $1 < n \leq 5$ . (ref. 12–17). In particular, tetragermane  $\text{Ge}_4\text{H}_{10}$  has enabled the growth of Ge-on-Si buffer layers at 330–360 °C with optimal growth rates and crystallinity. Mixtures containing  $\text{Ge}_4\text{H}_{10}$  diluted with  $\text{H}_2$  are used as flux to deposit the Ge films on Si at  $10^{-4}$ – $10^{-5}$  torr pressures and 360 °C temperature. Layer-by-layer growth takes place, leading to the formation of atomically flat, high purity films with optimized low-dislocation densities in the  $\sim 10^6 \text{ cm}^{-2}$  range and large thicknesses of at least 3  $\mu\text{m}$ , making the compound a very **effective** single-source precursor for Ge-based epitaxy at low temperatures (Fig. 1).

Fig. 1



The heavier polygermanes were also found much more compatible with Sn-sources than  $\text{GeH}_4$  when it came to the growth of  $\text{Ge}_{1-y}\text{Sn}_y$  alloys. The first reported CVD growth of  $\text{Ge}_{1-y}\text{Sn}_y$  used  $\text{Ge}_2\text{H}_6$  as the Ge-source,<sup>12,18</sup> and subsequent advances demonstrated the convenience of utilizing  $\text{Ge}_3\text{H}_8$  (ref. 13) and  $\text{Ge}_4\text{H}_{10}$  (ref. 14–16) to enable the growth of alloys with continuous Sn contents from 0.05% to 36% Sn. This extended compositional range is obtained by lowering the reaction temperature to levels in the range of 360–190 °C, mimicking MBE conditions. Such feat is not achievable with other CVD approaches.

The only significant drawback of the polygermane approach to the low-temperature growth of Ge-based compounds is the lack of a direct synthesis route to these precursors.  $\text{Ge}_2\text{H}_6$  is a byproduct of the industrial synthesis of  $\text{GeH}_4$  by hydrolysis of germanium oxide,<sup>2</sup> ~~and recent refinements to improve the  $\text{GeH}_4$  yield have purposely reduced the residual amounts of  $\text{Ge}_2\text{H}_6$  in production lines~~. This, combined with the increased niche demand for  $\text{Ge}_2\text{H}_6$ , has led to a dramatic increase in price to about US\$ 75 per gram. Supply-chain issues have put additional pressures on the availability and pricing of  $\text{Ge}_2\text{H}_6$  as of late. The synthesis of  $\text{Ge}_4\text{H}_{10}$  adds another layer of complication since this compound is obtained as a side product from the thermolysis reaction of  $\text{Ge}_2\text{H}_6$  in a flow reactor. An open challenge for applications is the production of sufficient amounts of  $\text{Ge}_4\text{H}_{10}$  *via* this method to meet increased demand for the fabrication of optical devices on Si. These circumstances motivate the interest in developing cheaper and more easily obtainable alternatives to polygermanes. Very recently, Lai *et al.* demonstrated PECVD growth of Ge on Si at 450 °C using  $\text{GeCl}_4$  as the Ge source. In this study, we explore the deployment of  $\text{GeH}_3\text{Cl}$  as a Ge precursor for low-temperature deposition of Ge and GeSn for the first time.<sup>19</sup>

Although chlorosilanes such as  $\text{SiHCl}_3$  and  $\text{SiH}_2\text{Cl}_2$  have been employed for SiGe, SiC and SiGeC fabrication, chlorogermanes in the general class of  $\text{GeH}_{4-n}\text{Cl}_n$  ( $n = 1\text{--}3$ ) compounds have attracted virtually no attention for group IV epitaxy.<sup>20</sup>  $\text{GeH}_3\text{Cl}$  is the simplest most volatile member in this class, and it is attractive for CVD applications due to its favorable chemical and physical properties. Its low boiling point (28 °C) and its high vapor pressure of  $\sim 530$  torr at room temperature provide flexibility in processing conditions and ease of delivery. The high volatility is a significant advantage over  $\text{Ge}_4\text{H}_{10}$ , making the compound more versatile for applications in variable-pressure CVD spanning from atmospheric to ultra-high vacuum chemical vapor deposition (UHV-CVD). In contrast,  $\text{Ge}_4\text{H}_{10}$  is a high boiling point liquid with a vapor pressure of 1 torr, which limits its applications to low-pressure conditions.  $\text{GeH}_3\text{Cl}$  is not pyrophoric or explosive in air and reacts slowly with  $\text{H}_2\text{O}$ , allowing convenient handling and storing.

The results reported in this paper are encouraging as we were able to grow thick, bulk-like Ge layers, with a structural quality comparable to  $\text{Ge}_4\text{H}_{10}$ -based growths. We have also been able to dope these materials using our standard battery of low-temperature precursors and fabricate Ge diodes with an optical responsivity that exceeds that obtained with similar  $\text{Ge}_4\text{H}_{10}$ -based devices. Furthermore, we have demonstrated ultralow temperature synthesis of  $\text{Ge}_{1-y}\text{Sn}_y$  alloys by combining  $\text{GeH}_3\text{Cl}$  and  $\text{SnD}_4$ . Initial experiments to test the limits of Sn incorporation using this precursor have produced films with Sn concentrations approaching 5%.

## 2. Growth experiments

### 2.1. Synthesis of $\text{GeH}_3\text{Cl}$

$\text{GeH}_3\text{Cl}$  is prepared by mixing neat  $\text{GeH}_4$  and  $\text{SnCl}_4$  at room temperature without the need of organic solvents that could introduce undesirable impurities.<sup>21</sup> We utilize the  $\text{GeH}_4$  byproduct recycled from the pyrolysis of  $\text{Ge}_2\text{H}_6$  to make  $\text{GeH}_3\text{Cl}$ . This economical recycling of Ge byproducts by our lab ensures no net loss of expensive and rare Ge. Eqn (1) summarizes the reaction process. No secondary  $\text{GeH}_2\text{Cl}_2$  phase or  $\text{GeHCl}_3$  is formed, indicating a single reaction pathway leading to efficient conversion of  $\text{GeH}_4$  to the target product.



The  $\text{SnCl}_2$  byproduct is an involatile solid allowing straightforward separation from the volatile components of the reaction mixture.  $\text{GeH}_3\text{Cl}$  is isolated as a colorless mobile liquid in high yields ranging from 56–88% in our hands. The yield is enhanced over this range by increasing the  $\text{GeH}_4$  pressure in the reaction mixture. The typical amount of  $\text{GeH}_3\text{Cl}$  produced in our experiments vary from 2.5 to 7 grams. The compound is purified from  $\text{HCl}$  by distillations to ensure a semiconductor-grade product. Its identity is established by IR spectroscopy and vapor pressure measurements following the method reported in ref. 21.  $\text{GeH}_3\text{Cl}$  has been used routinely in the past as a starting material for the synthesis of other  $\text{GeH}_3$  derivatives, including the  $\text{P}(\text{GeH}_3)_3$ ,  $\text{As}(\text{GeH}_3)_3$  and  $\text{Sb}(\text{GeH}_3)_3$  CVD precursors that are currently employed for n-type doping of group-IV semiconductors.

## 2.2. Ge growth

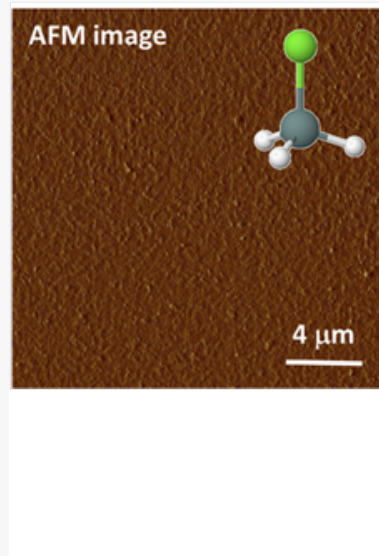
We initially explored the potential of  $\text{GeH}_3\text{Cl}$  for CVD applications by depositing intrinsic and doped Ge layers on Si. An important outcome is that the experiments consistently produced highly oriented crystals with smooth mirror-like surfaces and no sign of imperfections introduced during growth, such as extended defects and haze. This demonstrates the practicality of the compound for the fabrication of good crystal quality samples. The growths were conducted in a gas-source molecular epitaxy reactor (GSME) with base pressure of  $10^{-10}$  torr and operating at temperatures  $T < 400$  °C and pressures  $P \sim 10^{-4}$ – $10^{-7}$  Torr. The substrates were RCA-cleaned, 4" Si(100) wafers doped with B, exhibiting nominal resistivities in the 10–20  $\Omega$  cm range. Prior to growth the wafers were dipped in HF/methanol solutions to hydrogen-passivate the surface and then blown dried with a nitrogen nozzle. The wafers were then loaded into the reactor and degassed at 450 °C under UHV conditions. They were flashed at 900 °C to desorb residual contaminants and generate an epi-ready surface.

A glass ampule containing gaseous aliquots of pure  $\text{GeH}_3\text{Cl}$  was attached to the injection manifold. The pure and undiluted vapor of the compound was released into the chamber through the manifold using a high precision needle valve and allowed to flow over the substrate surface. The pressure inside the chamber was adjusted to  $5 \times 10^{-5}$  torr and was kept constant at this level throughout each run. Initial experiments were conducted at 330 °C, producing mirror-like films with 500 nm thickness. Subsequent trials focused on producing a series of samples by varying the temperature between 330–370 °C, a range that is broader than the 360–380 °C temperature window typically used for  $\text{Ge}_4\text{H}_{10}$ . The objective was to test the limits of the reactivity of  $\text{GeH}_3\text{Cl}$  and to determine the conditions for achieving reasonable growth rates and sample thicknesses without compromising sample quality. The film thicknesses ranged from 300 nm to 800 nm depending on the growth time. We found that the growth rate gradually increased, from 2 nm  $\text{min}^{-1}$  at 330 °C to 9–10 nm  $\text{min}^{-1}$  at 370 °C, irrespective of final thickness. The latter are nearly half of those observed for  $\text{Ge}_4\text{H}_{10}$  at the same growth temperature. This may be due to the lower pressures (by an order of magnitude) employed for  $\text{GeH}_3\text{Cl}$ . Attempts to grow samples at 380 °C generated rough and hazy films, indicating that small temperature shifts above the optimal limit had an impact on surface morphology and defectivity. We note that the substrates in this study are heated by radiant energy emitted from a resistance heater. The temperatures quoted in this paper correspond to those of the heater. The actual substrate temperatures are typically  $\sim 20$  °C lower. The heater is enclosed in a differentially pumped quartz jar positioned 2 mm away from the backside of the wafer inside the chamber (see ESI<sup>†</sup> for details). Under these conditions, we found that smaller size or conductive substrates are heated more efficiently than the full 4" wafers or resistive analogs. As a result, at any given nominal temperature we observe significantly higher growth rates on quadrants of 4" Si wafers than on the intact counterpart, *e.g.*  $\sim 8$  nm  $\text{min}^{-1}$  vs. 2 nm at 330 °C. The rates observed here are sufficiently high to produce the desired film thicknesses at comparable temperature to  $\text{Ge}_4\text{H}_{10}$ .

Spectroscopic ellipsometry was used to estimate layer thicknesses and determine carrier concentrations of Ge layers. AFM images of as-grown layers were obtained to measure morphology. Large area 20–20  $\mu\text{m}^2$  scans revealed featureless and flat surfaces with an RMS roughness of  $\sim 1$ –1.5 nm as shown in Fig. 2. High resolution X-ray diffraction (XRD) was used to characterize crystallinity and evaluate layer alignment with Si. On-axis XRD plots revealed strong and sharp 004 reflections, as shown in Fig. 3 for a 475 nm film. The FWHM of a typical rocking curve was 0.065°, or 235 arc-seconds, indicating a narrow spread of crystal mosaics. Off-axis 224 reciprocal space maps revealed narrow and symmetrical peaks corresponding to bulk Ge devoid of any significant strain or distortions induced by the lattice misfit of the film with the Si wafer. Further structural characterizations were conducted using a JEOL ARM 200F atomic resolution microscope with 200 kV operating voltage. Bright field (BF) and medium angle annular dark field (MAADF) images in STEM mode revealed uniform and monocrystalline layers. A MAADF strain-contrast

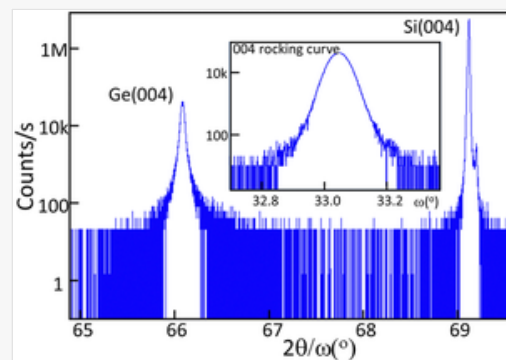
image of a  $\sim 500$  nm thick film is presented in Fig. 4(a) indicating the presence of defects shown as bright features near the interface region. A survey of images across the entire cross sectional specimen only showed occasional threading defects in the bulk layer with large segments of the layer appearing defect free. A high resolution  $z$ -contrast image is shown in Fig. 4(b) illustrating that the surface of the film is atomically smooth within the field of view.

Fig. 2



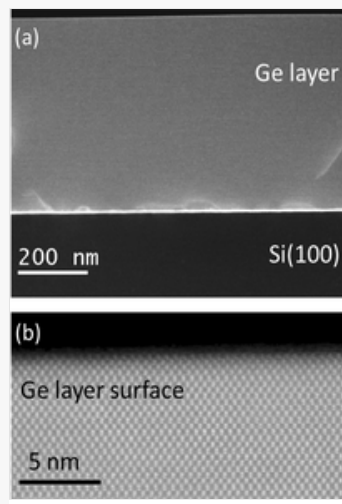
$20 \times 20 \mu\text{m}^2$  AFM image of a 475 nm thick Ge film grown on Si. The surface RMS roughness is  $\sim 1$  nm.

Fig. 3



High resolution XRD spectra for a Ge-on-Si sample showing a typical on-axis plot of the 004 peaks for the Ge layer and Si wafer. Inset shows the 004 rocking curve of the sample.

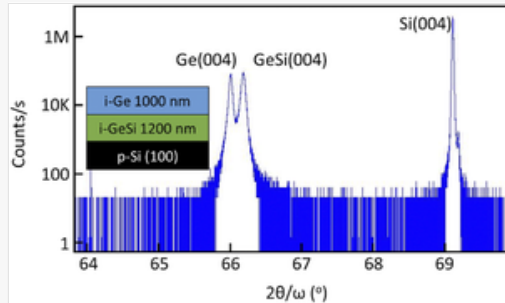
Fig. 4



XTEM images of a 500 nm thick Ge film on Si. The MAADF image in panel (a) shows good crystallinity and morphology. Dislocation loops are at the interface region. The z-contrast atomic resolution image in panel (b) reveals a flat layer surface.

Although the above films were grown directly on Si, several test growths were also performed on  $\text{Ge}_{1-x}\text{Si}_x$  buffered Si ( $x = 0.03$ ). The motivation for testing  $\text{Ge}_{1-x}\text{Si}_x$  buffer layers is the subsequent fabrication of backside-illuminated diodes grown on Si (future work) with enhanced responsivity at 1550 nm. Fig. 5 shows an XRD plot for a 1.0  $\mu\text{m}$  thick layer of Ge grown on a 1200 nm thick GeSi buffer layer. The Ge film was grown at 350  $^{\circ}\text{C}$  and  $5.0 \times 10^{-5}$  torr with a growth rate of 8 nm min $^{-1}$ . The sharp XRD peak profile corresponds to the “as-grown” sample, indicating superior crystallinity due to nearly lattice matched growth on the  $\text{Ge}_{1-x}\text{Si}_x$  platform.

Fig. 5



High resolution XRD spectra (004) of a 1  $\mu\text{m}$ -thick layer of Ge on GeSi grown using  $\text{GeH}_3\text{Cl}$ .

To study the electrical properties of the Ge films, we grew samples on high-resistivity Si substrates for subsequent characterization *via* the Hall effect. From those measurements (assuming a Hall factor equal to unity), we find that the nominally intrinsic films are p-type with a carrier concentration  $p \sim 2 \times 10^{16} \text{ cm}^{-3}$ . This is about one order of magnitude less than the carrier concentrations found in Ge layers grown with the  $\text{Ge}_4\text{H}_{10}$  precursor, which are also p-type. The lower unintentional carrier concentration may explain the higher responsivity of  $\text{GeH}_3\text{Cl}$ -based diodes, as discussed below.



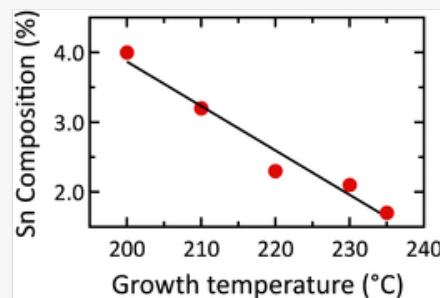
Doping the Ge layers with P atoms has enabled the fabrication of pin diodes, allowing further evaluation for device applications by measuring the electrical properties and optical response. Initially proof-of-concept single n-type layers were grown on Si(100) *via* reactions of  $\text{GeH}_3\text{Cl}$  and  $\text{P}(\text{SiH}_3)_3$  to investigate conditions for effective doping with P atoms. In a typical run  $\sim 5\%$   $\text{P}(\text{SiH}_3)_3$  reagent is used by volume. The depositions were conducted at  $360^\circ\text{C}$  and  $5 \times 10^{-5}$  torr yielding mirror-like flat films. High resolution XRD revealed epitaxial Ge layers with excellent crystallinity exhibiting a cubic lattice constant of  $5.658 \text{ \AA}$ , virtually identical to that measured for intrinsic Ge, which indicates no significant Si incorporation from the  $\text{SiH}_3$  groups of the  $\text{P}(\text{SiH}_3)_3$  precursor under these conditions. Phosphorus carrier concentrations of  $1\text{--}2 \times 10^{19} \text{ cm}^{-3}$  were measured by IR ellipsometry. The latter also revealed layer thicknesses of about 475–500 nm for a typical run.

### 2.3. GeSn growth

Next, we explored the feasibility of synthesizing  $\text{Ge}_{1-y}\text{Sn}_y$  alloys by reactions of  $\text{GeH}_3\text{Cl}$  with  $\text{SnD}_4$  as the source of Sn. Our proof-of-concept experiments were conducted in the same GSME reactor employed for the Ge depositions described above. Four inch Si wafers incorporating 4350–500 nm-thick Ge buffer layers were used as substrates. These were first wet-cleaned and then flashed on the sample stage at  $650^\circ\text{C}$  to remove impurities from the surface prior to growth. Appropriate amounts of pure  $\text{SnD}_4$  and  $\text{GeH}_3\text{Cl}$  gaseous samples were placed in separate containers and attached to different gas inlets of the GSME chamber, allowing independent adjustment of each precursor gas flow into the reactor. In a typical run, the  $\text{GeH}_3\text{Cl}$  vapor was introduced first into the chamber, and the flow rate was adjusted to set the pressure at  $4 \times 10^{-5}$  torr the inside the reactor. The  $\text{SnD}_4$  vapor was injected next, further raising the pressure to a final cumulative  $6 \times 10^{-5}$  torr threshold that was kept constant during the run by continuous pumping of the chamber contents with a turbomolecular pump. A series of growth trials was performed under these conditions by varying the reaction temperature from  $200^\circ\text{C}$  to  $235^\circ\text{C}$ . This allowed us to obtain insights into the reactivity behavior of  $\text{GeH}_3\text{Cl}$  with the Sn source and explore Sn incorporation possibilities under ultra-low temperatures akin to MBE.

The initial reactions at  $200^\circ\text{C}$  produced samples with  $\sim 4\%$  Sn substitution. Raising the temperature to  $210^\circ\text{C}$  yielded samples with a lower Sn content of 3.2%. The Sn incorporation decreased even further with increasing temperature as shown in in Fig. 6. The trend toward lower Sn contents as the temperature is increased is consistent with prior results obtained from reactions of  $\text{Ge}_4\text{H}_{10}$  with  $\text{SnD}_4$ .

Fig. 6

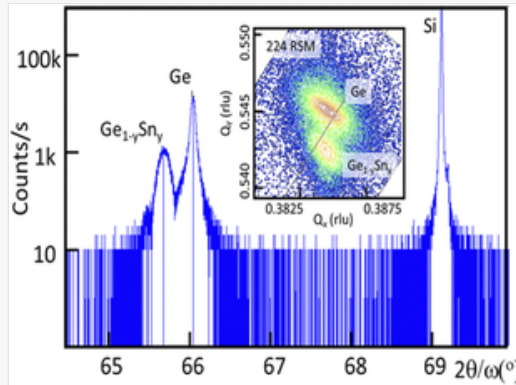


Sn concentration vs. growth temperature for representative samples grown by GSME showing a decrease in Sn content with increasing temperature grown using  $\text{GeH}_3\text{Cl}$ .

All samples produced in this preliminary study exhibited smooth, mirror-like surfaces devoid of defects and imperfections. Their structures were found to be monocrystalline, epitaxial, and fully strained to the Ge template as evidenced by XRD characterizations. Fig. 7 shows representative plots for a sample with 2.1% Sn and 54 nm thickness grown on a 366 nm thick Ge buffer. The on-axis scan shows (004) peaks for the  $\text{Ge}_{1-y}\text{Sn}_y$  film, the Ge buffer, and the substrate. A RSM shows 224 peaks for the buffer and the epi-layer. The in-plane (*a*) and vertical (*c*) lattice parameters

under the stress-induced tetragonal distortion were determined from these XRD data for all  $\text{Ge}_{1-y}\text{Sn}_y$  films and used to calculate their relaxed cubic parameter ( $a_0$ ) using linear elasticity theory. The Sn contents were then obtained using Vegard's law.<sup>22</sup> We note that the XRD Sn compositions in our GeSn samples have been calibrated using RBS and this enables accurate determination of substitutional Sn.<sup>22</sup> For the sample in Fig. 7 the RSM reveals a full compressive strain of  $-0.122\%$  in the  $\text{Ge}_{1-y}\text{Sn}_y$  layer and a residual  $+0.138\%$  tensile strain in the Ge buffer.

Fig. 7



XRD plots showing 004 peaks (blue line) and 224 RSM (inset) for a 2.1% Sn sample grown on a Ge buffer. The relaxation line passes slightly below the buffer peak indicating the presence of a slight in plane tensile strain due to ~~due~~ annealing at 550 for 60 seconds prior to GeSn growth. The  $\text{Ge}_{1-y}\text{Sn}_y$  peak lies below the relaxation line and aligns with the Ge peak in the vertical direction, indicating that the alloy layer is compressively strained and essentially unrelaxed relative to the Ge buffer.  $Q_x$  and  $Q_y$  are measured in reciprocal lattice units (rlu).  $Q_y(001) = (2\lambda/c)$  where  $\lambda = 1.5405 \text{ \AA}$  and  $c$  is the lattice parameter along the growth direction.  $Q_x(110) = \lambda\sqrt{2}/a$  where  $a$  is the in-plane lattice parameter.

We emphasize here that the growth temperatures for  $\text{Ge}_{1-y}\text{Sn}_y$  alloys are lower than those needed for pure Ge growth by at least  $100^\circ\text{C}$ . When examined separately, neither  $\text{SnD}_4$  nor  $\text{GeH}_3\text{Cl}$  will decompose to generate any noticeable film growth at the temperatures employed in this study, suggesting a cooperative growth mechanism.

Additional preliminary depositions were pursued to further explore the synthetic potential of the  $\text{GeH}_3\text{Cl}/\text{SnD}_4$  system using in this case a hot wall CVD reactor that operates at higher pressures than the GSME system. The tubular hot walls of the reactor facilitate activation of the CVD reagents, induce gas phase reactions that enable Sn substitution at much higher temperatures and enhance the growth rates, leading to thicker films. The initial gas phase stoichiometry of the precursors was selected to be  $\sim 5\%$   $\text{SnD}_4$  and  $95\%$   $\text{GeH}_3\text{Cl}$  diluted with large amounts of high purity  $\text{H}_2$ . The combined flux was then admitted into the reactor through mass flow controllers at 0.2 torr background pressure, established by a continuous flow of  $\text{H}_2$ . Under these conditions, films with smooth surfaces approaching 100 nm thickness were grown at  $305^\circ\text{C}$  and  $310^\circ\text{C}$  on quadrants of 4" Si wafers. XRD analysis of the samples revealed monocrystalline and hetero-epitaxial  $\text{Ge}_{1-y}\text{Sn}_y$  alloys fully strained to the underlying Ge template. The Sn concentration was determined by XRD to be in the range of 4–4.5%, closely matching the 5% gas phase concentration of  $\text{SnD}_4$  in the reaction zone. This outcome portends the prospect for composition control and the ability to design the film stoichiometry, mitigating waste of excess Ge. The favorable preliminary results indicate that extending the compositional range beyond the SWIR range to materials with direct gaps may be within reach and will part of future synthetic work.

### 3. Growth mechanisms

Growth studies using  $\text{GeH}_4$  and  $\text{Ge}_2\text{H}_6$  have demonstrated that dehydrogenation is initiated *via* a single-hydrogen elimination reaction.<sup>23–25</sup> In the case of  $\text{GeH}_4$ , the subsequent transfer of an additional H atom to an empty surface site leaves a  $\text{GeH}_2$  fragment that induces a cleavage of the dimer to which it attached and inserts itself as a bridging unit. This is the crucial step by which Ge is incorporated into the growing film.  $\text{Ge}_2\text{H}_6$  follows a similar reaction path until a  $\text{GeH}_2\text{GeH}_2$  double group inserts itself between two surface dimers. The key intermediate species in both cases is  $\text{GeH}_2$ —with preferred  $\text{Ge(II)}$  oxidation state—rather than unstable  $\text{GeH}_3$  radicals. The decomposition mechanisms of  $\text{Ge}_3\text{H}_8$  and  $\text{Ge}_4\text{H}_{10}$  have not been experimentally or theoretically studied to date and the reaction intermediates have not been identified to our knowledge. However, based on their molecular structures and observed growth behavior in

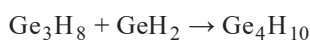


our hands, we can qualitatively predict the formation of multiple  $\text{GeH}_2$  fragments, which can then serve as the enabling building blocks for Ge crystal assembly. Gaseous  $\text{Ge}_4\text{H}_{10}$  comprises the branched  $\text{GeH}(\text{GeH}_3)_3$  and linear  $\text{GeH}_3\text{GeH}_2\text{GeH}_2\text{GeH}_3$  isomers at the growth temperatures. The linear isomer may interact with the surface in a similar manner to  $\text{Ge}_2\text{H}_6$ , with several points of contact including the terminal  $\text{GeH}_3$  ligands as well as the central  $-\text{GeH}_2\text{GeH}_2-$  core. The branched isomer is 80% abundant and thus dominant at the growth front. Here the possibilities are varied. A simple path would be decomposition  $\text{Ge}_4\text{H}_{10}(\text{g}) \rightarrow \text{Ge}_3\text{H}_8(\text{g}) + \text{GeH}_2(\text{a})$ , where the trigermane would subsequently react with the surface to deliver additional Ge atoms to the growth front. This reaction has been proposed for neopentasilane-based growth.<sup>26</sup>

The key  $\text{GeH}_2$  groups can also be generated *via* homogeneous decomposition in the gas phase. For  $\text{GeH}_4$ , for example, the mechanism discussed in the literature follows the reaction  $\text{GeH}_4(\text{g}) \rightarrow \text{GeH}_2(\text{g}) + \text{H}_2(\text{g})$ . For  $\text{Ge}_2\text{H}_6$ , the well-established process  $\text{Ge}_2\text{H}_6(\text{g}) \rightarrow \text{GeH}_2(\text{g}) + \text{GeH}_4(\text{g})$  at  $T \sim 250^\circ\text{C}$  could also yield highly reactive  $\text{GeH}_2$  fragments. In fact, the generation of these fragments is a critical step for the synthesis of higher order germanes *via* the insertion reactions

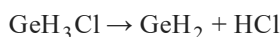


2



3

In the case of  $\text{GeH}_3\text{Cl}$ , we suggest that homogeneous decomposition might be promoted by eliminating highly robust HCl-leaving groups according to



4

This process is facilitated by the asymmetry and bond polarity imbued by replacing H with Cl in tetrahedral  $\text{GeH}_4$ . This reaction generates—in a single step and without further activation—the  $\text{GeH}_2$  reactive intermediate that can lead to the growth of Ge-based materials. To gain more insight into the decomposition mechanism of  $\text{GeH}_3\text{Cl}$ , we conducted a model experiment to study the thermal behavior of the compound. The compound vapor diluted with  $\text{H}_2$  carrier gas in a bubbler was passed through a flow tube at  $\sim 280^\circ\text{C}$  and one atmosphere pressure for 45 minutes. The gaseous byproducts were collected in a liquid nitrogen trap and analyzed by FTIR, revealing predominately HCl. This is consistent with [eqn \(4\)](#).

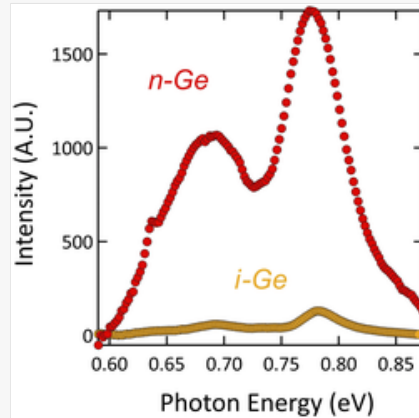
The observation that the growth of  $\text{Ge}_{1-y}\text{Sn}_y$  using  $\text{GeH}_3\text{Cl}/\text{SnD}_4$  proceeds at temperatures much lower than those needed to grow pure Ge films with the same  $\text{GeH}_3\text{Cl}$  Ge-source is perfectly consistent with our observations using polygermanes. For example, optical quality  $\text{Ge}_{1-y}\text{Sn}_y$  films are grown at  $\sim 190$ – $210^\circ\text{C}$  using  $\text{Ge}_4\text{H}_{10}$ , well below the  $330$ – $360^\circ\text{C}$  range that provides optimal pure Ge growth. The fact that tangible films are produced at lower temperatures when the Ge- and Sn-precursors are combined indicates that the growth mechanism involves a cooperative chemical interaction of the compounds. Previous studies have shown that  $\text{GeH}_4$  and  $\text{SiH}_4$  react together to produce  $\text{Si}_{1-x}\text{Ge}_x$  alloys,<sup>27,28</sup> and this can occur at lower temperatures than the thermal dehydrogenation of  $\text{SiH}_4$ . The prevailing explanation is that the H atoms at the growth front migrate from Si to Ge surface sites, where they are released more easily as  $\text{H}_2$  due to the fact the Ge–H bonds are weaker than Si–H. The same trend has been observed when  $\text{Ge}_2\text{H}_6$  or  $\text{Ge}_4\text{H}_{10}$  are reacted with  $\text{SnH}_4$  to produce  $\text{Ge}_{1-y}\text{Sn}_y$  using CVD. In our study we envision that a transfer of H from Ge to the heavier Sn may occur on the surface, facilitating H desorption due to the low thermal stability of Sn–H bonds. An alternative mechanism may involve direct reactions between  $\text{GeH}_3\text{Cl}$  and  $\text{SnD}_4$ , creating short-lived unstable intermediates that subsequently condense on the surface. In order to probe further and in an effort to gauge the reactivity of the  $\text{SnD}_4$  and  $\text{GeH}_3\text{Cl}$ , we combined gas phase aliquots of the latter with the former at 5% by volume in a glass litter flask. We observed an immediate reaction taking place at room temperature as evidenced by the formation of a film residue on the glass walls of the flask. This behavior is not observed when  $\text{SnD}_4$  is mixed with  $\text{Ge}_2\text{H}_6$ , or  $\text{Ge}_3\text{H}_8$  and  $\text{Ge}_4\text{H}_{10}$ , suggesting that  $\text{GeH}_3\text{Cl}$  reacts readily with stannane at room temperature.

## 4. Optical characterization

## 4.1. Photoluminescence

To further characterize the quality of the Ge layers we compared the room temperature photoluminescence (PL) spectra of selected n-type and intrinsic samples. Ge films are known to exhibit significant direct gap photoluminescence,<sup>29</sup> and the PL intensity can be further enhanced by populating the conduction band with electrons through n-doping.<sup>30</sup> The PL spectra were collected using a custom system comprising of a 980 nm laser with 200 mW net output power, a chopper that provides modulation, a 1064 nm long-pass filter, a lock-in amplifier, a Horiba MicroHR spectrometer, and a liquid nitrogen-cooled InGaAs detector. A typical sample was subjected to rapid thermal annealing (RTA) treatments at 650 °C three times for two seconds each time. XRD showed a slight tensile strain and ellipsometry indicated identical carrier concentrations relative to the as grown samples. Fig. 8 shows a PL spectrum for an annealed Ge:P film with  $n = 1.1 \times 10^{19} \text{ cm}^{-3}$  and a thickness of 475 nm. The peaks are strong and well-defined, exhibiting line shapes consistent with those observed from analogous n-type samples produced using  $\text{Ge}_4\text{H}_{10}$ . The strongest peak at 0.775 eV, corresponds to direct gap emission and the second, lower intensity peak at  $\sim 0.69$  eV is assigned to phonon-assisted indirect gap emission. The overall line shape is very similar to that observed in bulk Ge,<sup>31</sup> except for the well-known fact that in films the direct emission is enhanced due the smaller role played by self-absorption.<sup>29</sup> The peak energies are slightly downshifted relative to the bulk, which reflects the combined effect of tensile strain and band-gap renormalization.<sup>32</sup> The spectrum of the n-type film is compared in Fig. 8 with that of an intrinsic, 2400 nm thick, Ge film grown by  $\text{Ge}_4\text{H}_{10}$  showing that the intensity is much higher and confirming a high level of activation of the dopants. The quality of the optical response provides further evidence on the ability of the  $\text{GeH}_3\text{Cl}$  approach to yield device-quality doping layers under the low thermal processing conditions in our experiments.

Fig. 8



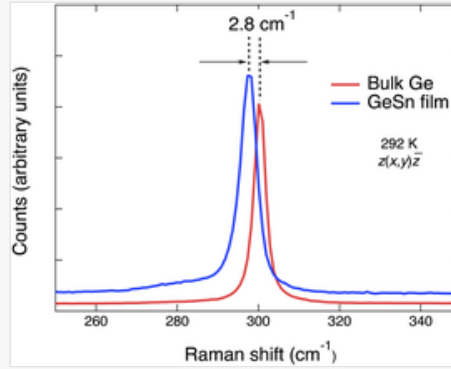
Room-temperature photoluminescence spectrum (red dots) for a 475 nm Ge-layer doped n-type with  $1.1 \times 10^{19} \text{ atoms cm}^{-3}$ . The main peak at 0.775 eV is assigned to direct-gap emission, and the secondary peak at 0.69 eV is assigned to phonon-assisted indirect gap emission. Spectrum of an undoped 2400 nm Ge layer grown using  $\text{Ge}_4\text{H}_{10}$  showing that the signal is very weak in this scale in spite of its much larger thickness.

## 4.2. Raman spectroscopy

Fig. 9 shows Raman spectra for a  $\text{Ge}_{1-y}\text{Sn}_y$  film and for bulk Ge. The spectra were obtained with 514 nm excitation. At this wavelength, the optical absorption in the film is so high that the buffer layer is not sampled. The observed peak corresponds to the zone-center three-fold degenerate optical phonon for the diamond structure. We observe a downshift of about  $2.8 \text{ cm}^{-1}$  in the peak frequency of the alloy relative to the film. This shift is given by  $\Delta\omega = \alpha y + b\varepsilon_{\parallel}$ , where  $\varepsilon_{\parallel}$  is the in-plane strain. Using  $\alpha = -78 \text{ cm}^{-1}$  (ref. 15) and  $b = -415 \text{ cm}^{-1}$  (ref. 33) and the measured compressive strain  $\varepsilon_{\parallel} = -0.33\%$ , we estimate a Sn concentration  $y = 5.4\%$ . This is higher than the Sn concentration  $y = 3.2\%$  obtained from the X-ray analysis. Raman measurements for another sample with  $y = 3.8\%$  from X-rays, give  $y = 5.7\%$ , so that the trend is reproduced, but the absolute value is clearly higher. We note, the coefficients  $\alpha$  and  $b$  have been determined mainly from measurements of samples with  $y > 5\%$ , and the linearity of the relationship at low concentrations is not definitively established. Anomalies in the compositional dependence of modes at very low alloy concentrations have been reported in the Si-Ge system and might appear in the Ge-Sn system as well.<sup>34</sup> As indicated above the Sn contents obtained by HRXRD are calibrated by RBS. The discrepancy with the Raman likely lies with

the modelling of the spectra. We note that to ensure compositional uniformity of the samples we obtained XRD spectra throughout the wafer surface and all measurements were essentially identical.

Fig. 9

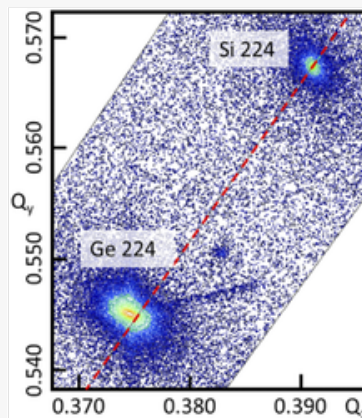


Raman spectrum of a  $\text{Ge}_{1-y}\text{Sn}_y$  film compared with the Raman spectrum of a bulk Ge sample. Both spectra are collected at room temperature. The scattering configuration is indicated in the Porto notation, with  $x, y, z$  being the Cartesian directions in the cubic lattice.

## 5. Device fabrication and characterization

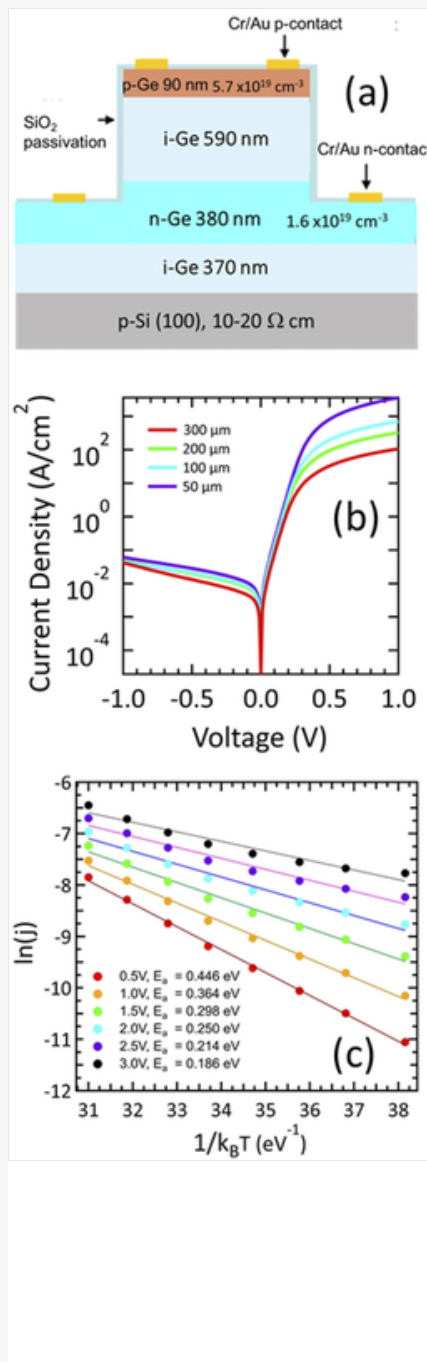
The ability to dope prompted us to explore the feasibility of fabricating prototype pin photodiodes and measure their IV curves and spectral responsivities. The objective was to further characterize the Ge materials produced using  $\text{GeH}_3\text{Cl}$  from a device fabrication perspective. We adopted a simple homostructure design comprising a/n-Ge/i-Ge/p-Ge stack grown on a Ge-buffered Si platform. The Ge buffer was grown first with 370 nm thickness and was annealed *in situ* to optimize crystallinity and remove any residual strains. The n-layer (thickness  $t = 380$  nm,  $n = 1.6 \times 10^{19} \text{ cm}^{-3}$ ) and the intrinsic Ge layer ( $t = 590$  nm) were then grown following each other in succession without removing the sample from the chamber. The p-Ge capping layer ( $t = 90$  nm,  $p = 5.7 \times 10^{19} \text{ cm}^{-3}$ ) was grown *ex situ* using a CVD reactor specifically calibrated for doping the samples with B atoms using  $\text{B}_2\text{H}_6$ . The layers were deposited following protocols described above and their thicknesses and carrier concentrations were measure by ellipsometry. The n-i-p layers were not subjected to any thermal processing and were used “as-grown”. XRD spectra of the entire stack were measured and the on axis and off axis plots demonstrated single 004 and 224 Ge peaks (see Fig. 10) with sharp and narrow profiles corroborating the good crystal quality and seamless integration of the different layers in the stack.

Fig. 10



Circular mesa devices with diameters ranging from 300 to 50  $\mu\text{m}$  were patterned by photolithography. The mesas were then etched down to the n-Ge layer using a  $\text{BCl}_3$  plasma. They were passivated by depositing an  $\text{SiO}_2$  layer which also serves as an antireflection coating. Electrical metal contacts of Cr/Au were patterned by photolithography and then deposited by thermal evaporation. The schematic in Fig. 11(a) provides details of mesa sizes, electrical contacts, doping concentrations and thicknesses of the layers in the stack, including the Ge buffer. Current–voltage plots demonstrating diode behavior are shown in Fig. 11(b). The dark current densities at  $-1$  V reverse bias for 50–300  $\mu\text{m}$  devices are very close and fall in the  $4.2\text{--}6.1 \times 10^{-2} \text{ A cm}^{-2}$  range, which are comparable with of state-of-the-art values for  $\text{Ge}_4\text{H}_{10}$  diodes with similar homostructure designs. Activation energies were extracted from Arrhenius fits to the temperature dependence of the dark current, as shown in Fig. 11(c). They span energies ranging from 0.446 eV ( $\sim E_0/2$ ) to 0.186 eV, suggesting that the dark current is dominated by Shockley–Reed–Hall recombination with a contribution from trap-assisted tunneling.<sup>35</sup> The trap levels are normally assumed to be linked to threading dislocations, but we cannot rule out a contribution from point defects. Whatever the origin, the reverse bias currents are very similar to those observed in comparable devices fabricated with the  $\text{Ge}_4\text{H}_{10}$  precursor. For example, the 300  $\mu\text{m}$  device above gives a current density of  $4 \times 10^{-2} \text{ A cm}^{-2}$  at  $-1$  V, whereas a very similar diode fabricated with  $\text{Ge}_4\text{H}_{10}$  has a  $-1$  V current density of  $6 \times 10^{-2} \text{ A cm}^{-2}$ . This strongly suggests a similar concentration of defects for both growth approaches.

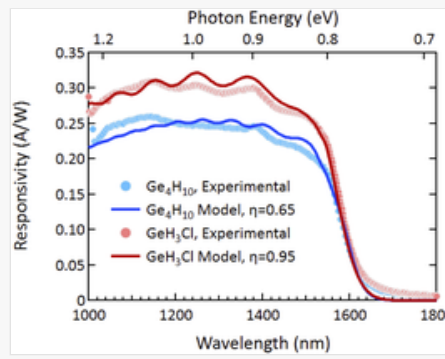
Fig. 11



(a) Schematic representation of the Ge pin device grown on Ge-buffered Si(100) showing layer thicknesses and doping concentrations. (b) Current–voltage plots of diodes with mesa diameters ranging from 50 μm to 300 μm. (c) Temperature dependence of the current at selected voltages between 0.5 V and 3.0 V.

The spectral responsivity of the diodes was measured at zero bias using monochromatized light generated from a tungsten lamp. The light was focused to a spot size of 50 μm onto the  $\text{SiO}_2$  window of the device. The generated photocurrent was then measured using a lock-in amplifier. The resultant responsivity spectrum is displayed in Fig. 12 for a 300 nm device, and it is compared with the responsivity from an analogous reference device produced using the  $\text{Ge}_4\text{H}_{10}$  approach. The latter devices also utilize homostructure stacks akin to those displayed in the figure and have a thicker active layer of 740 nm. The solid lines in the figure represent a theoretical model using a recently developed tool to simulate the effect of multiple reflections in the structure and the absorption in individual layers.<sup>36</sup> We notice that the spectral responsivity of the  $\text{GeH}_3\text{Cl}$  device is higher than that of  $\text{Ge}_4\text{H}_{10}$  device despite the larger thickness in the latter. The collection efficiency (internal quantum efficiency) of the  $\text{GeH}_3\text{Cl}$  device is  $\eta = 95\%$ , approaching the theoretical limit for an ideal diode, and it is much larger than the value  $\eta = 0.65\%$  measured for the  $\text{Ge}_4\text{H}_{10}$  reference device. This demonstrates an improvement in optical response of the Ge diode produced by the  $\text{GeH}_3\text{Cl}$  approach, likely a result of a lower levels of electrically active impurities generated with this growth method.

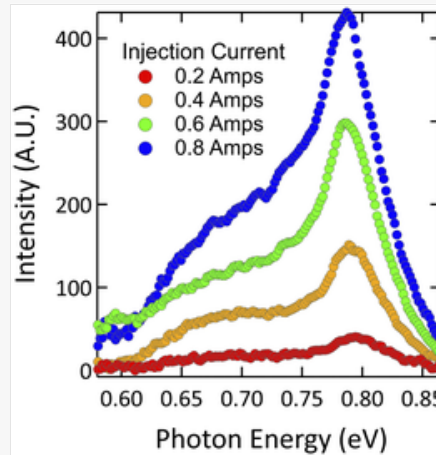
Fig. 12



Spectral responsivity for two Ge pin diodes grown with either  $\text{GeH}_3\text{Cl}$  or  $\text{Ge}_4\text{H}_{10}$  precursors as the source of Ge. The dotted lines are the experimental data, and the solid lines represent the theoretical fit. The cut off wavelengths for the  $\text{Ge}_4\text{H}_{10}$  and  $\text{GeH}_3\text{Cl}$  devices are 0.783 eV (1584 nm) and 0.780 eV (1579 nm) respectively. This is lower than the expected band gap energy of 0.80 eV for bulk Ge due to the slight tensile strain (0.121% and 0.124%, respectively) induced by the thermal processing of the buffer layers in both cases.

Fig. 13 shows electroluminescence spectra at room temperature obtained with the same system used to measure PL. Current was injected into a diode 500  $\mu\text{m}$  in diameter *via* probes from a current source. The current was pulsed at 50 Hz to be detected by the lock-in amplifier. The spectra look similar to the PL spectrum from a pure  $\text{GeH}_3\text{Cl}$  film, but the dip between direct gap and indirect gap peaks, clearly seen in Fig. 8, does not appear in Fig. 13. A possible reason is that in addition to the dominant direct gap emission from the intrinsic layer, there may be some direct gap emission from the heavily doped p and n layers, where the band gaps may be red-shifted by  $\sim 30$  meV due to renormalization effects. The corroboration of this conjecture will require detailed modeling of the EL spectrum.

Fig. 13



Room temperature electroluminescence from a Ge pin diode grown with the  $\text{GeH}_3\text{Cl}$  precursor. The spectra were collected for four different forward injection current currents ranging from 0.2 to 0.8 A.

## 6. Conclusions

In summary, we have demonstrated that chlorogermane  $\text{GeH}_3\text{Cl}$  is a viable precursor for the growth of device-quality Ge ~~and~~ films and good crystallinity GeSn alloys on Si substrates at ultra-low temperatures. The precursor retains the main advantage of heavy polygermanes—namely the ability to grow films at low temperatures compatible with CMOS processing and without the need of a two-step growth strategy to reduce defects—while being much easier to synthesize at a much lower cost. The Ge-layers grown with  $\text{GeH}_3\text{Cl}$  display structural and optical properties entirely comparable with those measured in films grown with  $\text{Ge}_4\text{H}_{10}$ , and better electrical properties that are likely the reason for a clear improvement in diode optical responsivity compared with devices fabricated using polygermanes.

## Author contributions

The manuscript was written through contributions of all authors. All authors have given approval to the final version of the manuscript. These authors (Matthew A. Mircovich and Aixin Zhang) contributed equally.



## Conflicts of interest

There are no conflicts to declare.

## Acknowledgements

This work was supported by the US National Science Foundation under grant DMR-2119583. We thank Dr Chi Xu for his contribution in the growth of the GeSi buffer layers.

## Notes and references



References can be edited in the panel that appears to the right when you click on a reference.

- 1 J. Margetis, S.-Q. Yu, B. Li and J. Tolle, *J. Vac. Sci. Technol., A*, 2019, **37**, [021508–1–8](#).
- 2 A. V. G. Chizmeshya, C. Ritter, J. Tolle, C. Cook, J. Menendez and J. Kouvetakis, *Chem. Mater.*, 2006, **18**, 6266–6277.
- 3 J. Xie, J. Tolle, V. R. D’Costa, C. Weng, A. V. G. Chizmeshya, J. Menendez and J. Kouvetakis, *Solid-State Electron.*, 2009, **53**, 816–823.
- 4 C. L. Senaratne, J. D. Gallagher, C. Xu, P. Sims, J. Menendez and J. Kouvetakis, *ECS Trans.*, 2015, **69**, 157–164.
- 5 C. Xu, J. D. Gallagher, P. M. Wallace, C. L. Senaratne, P. Sims, J. Menéndez and J. Kouvetakis, *Semicond. Sci. Technol.*, 2015, **30**, 105028.
- 6 C. Xu, C. L. Senaratne, P. Sims, J. Kouvetakis and J. Menendez, *ACS Appl. Mater. Interfaces*, 2016, **8**, 23810–23819.
- 7 C. Xu, P. M. Wallace, D. A. Ringwala, J. Menendez and J. Kouvetakis, *ACS Appl. Mater. Interfaces*, 2018, **10**, 37198–37206.
- 8 J.-H. Park, P. Kapur, K. C. Saraswat and H. Peng, *Appl. Phys. Lett.*, 2007, **91**, 143107.
- 9 J. Osmond, G. Isella, D. Chrastina, R. Kaufmann, M. Acciarri and H. V. Kanel, *Appl. Phys. Lett.*, 2009, **94**, 201106.
- 10 G. Dushaq, M. Rasras and A. Nayfeh, *Thin Solid Films*, 2017, **636**, 585–592.
- 11 B. Alharthi, J. M. Grant, W. Dou, P. C. Grant, A. Mosleh, W. Du, M. Mortazavi, B. Li, H. Naseem and S.-Q. Yu, *J. Electron. Mater.*, 2018, **47**, 4561–4570.
- 12 M. Bauer, J. Taraci, J. Tolle, A. V. G. Chizmeshya, S. Zollner, D. J. Smith, J. Menendez, C. Hu and J. Kouvetakis, *Appl. Phys. Lett.*, 2002, **81**, 2992–2994.
- 13 G. Grzybowski, R. T. Beeler, L. Jiang, D. J. Smith, J. Kouvetakis and J. Menéndez, *Appl. Phys. Lett.*, 2012, **101**, 072105.
- 14 L. Jiang, C. Xu, J. D. Gallagher, R. Favaro, T. Aoki, J. Menéndez and J. Kouvetakis, *Chem. Mater.*, 2014, **26**, 2522–2531.
- 15 C. Xu, P. M. Wallace, D. A. Ringwala, S. L. Y. Chang, C. D. Poweleit, J. Kouvetakis and J. Menéndez, *Appl. Phys. Lett.*, 2019, **114**, 212104.

- 16 C. Xu, D. Ringwala, D. Wang, L. Liu, C. D. Poweleit, S. L. Y. Chang, H. L. Zhuang, J. Menéndez and J. Kouvetakis, *Chem. Mater.*, 2019, **31**, 9831–9842.
- 17 C. Xu, T. Hu, D. A. Ringwala, J. Menéndez and J. Kouvetakis, *J. Vac. Sci. Technol., A*, 2021, **39**, [063411-1-12](#).
- 18 J. Taraci, J. Tolle, M. R. M. Cartney, J. Menendez, M. A. Santana, D. J. Smith and J. Kouvetakis, *Appl. Phys. Lett.*, 2001, **78**, 3607–3609.
- 19 J.-Y. Lai, S.-C. Tsai, M.-W. Lin and S.-Y. Chen, *Mater. Sci. Semicond. Process.*, 2022, **148**, [106740](#), DOI: [doi.org/10.1016/j.mssp.2022.106740](https://doi.org/10.1016/j.mssp.2022.106740).
- 20 J. L. Hoyt, T. O. Mitchell, K. Rim, D. V. Singh and J. F. Gibbons, *Thin Solid Films*, 1998, **321**, 41–46.
- 21 S. Cradock, M. A. Ring, P. Estacio and M. D. Sefcik, *Inorganic Syntheses*, 1974, 161–16410.1002/9780470132463.ch35
- 22 C. Xu, C. L. Senaratne, R. J. Culbertson, J. Kouvetakis and J. Menéndez, *J. Appl. Phys.*, 2017, **122**, 125702.
- 23 C.-S. Liu, L.-W. Chou, L.-S. Hong and J.-C. Jiang, *J. Am. Chem. Soc.*, 2008, **130**, 5440–5442.
- 24 C.-L. Cheng, D.-S. Tsai and J.-C. Jiang, *J. Phys. Chem. C*, 2007, **111**, 13466–13472.
- 25 D. Dick, J.-F. Veyan, R. C. Longo, S. McDonnell, J. B. Ballard, X. Qin, H. Dong, J. H. G. Owen, J. N. Randall, R. M. Wallace, K. Cho and Y. J. Chabal, *J. Phys. Chem. C*, 2013, **118**, 482–493.
- 26 K. H. Chung, N. Yao, J. Benziger, J. C. Sturm, K. K. Singh, D. Carlson and S. Kuppurao, *Appl. Phys. Lett.*, 2008, **92**, 113506.
- 27 B. S. Meyerson, K. J. Uram and F. K. LeGoues, *Appl. Phys. Lett.*, 1988, **53**, 2555–2557.
- 28 C. Li, S. John, E. Quinones and S. Banerjee, *J. Vac. Sci. Technol., A*, 1996, **14**, 170–183.
- 29 G. Grzybowski, R. Roucka, J. Mathews, L. Jiang, R. Beeler, J. Kouvetakis and J. Menéndez, *Phys. Rev. B: Condens. Matter Mater. Phys.*, 2011, **84**, 205307.
- 30 X. Sun, J. Liu, L. C. Kimerling and J. Michel, *Appl. Phys. Lett.*, 2009, **95**, 011911.
- 31 J. Menéndez, C. D. Poweleit and S. E. Tilton, *Phys. Rev. B: Condens. Matter Mater. Phys.*, 2020, **101**, 195204.
- 32 C. Xu, J. Kouvetakis and J. Menéndez, *J. Appl. Phys.*, 2019, **125**, 085704.
- 33 F. Cerdeira, C. J. Buchenauer, F. H. Pollak and M. Cardona, *Phys. Rev. B: Solid State*, 1972, **5**, 580.
- 34 H. D. Fuchs, C. H. Grein, M. I. Alonso and M. Cardona, *Phys. Rev. B: Condens. Matter Mater. Phys.*, 1991, **44**, 13120–13123.
- 35 B. Son, Y. Lin, K. H. Lee, Q. Chen and C. S. Tan, *J. Appl. Phys.*, 2020, **127**, [203105 1-9](#).
- 36 G. Timò, A. Martinelli and L. C. Andreani, *Prog. Photovoltaics Res. Appl.*, 2020, **28**, 27.

## Footnotes

## Queries and Answers

Q1

**Query:** Have all of the author names been spelled and formatted correctly? Names will be indexed and cited as shown on the proof, so these must be correct. No late corrections can be made.

**Answer:** Yes

Q2

**Query:** The Graphical Abstract text currently exceeds the space available for the published version. Please trim the text so that it is shorter than 250 characters (including spaces).

**Answer:** change made in the proof to comply with the 250 limit

Q3

**Query:** In the sentence beginning “Phosphorus carrier concentrations...”, please check that all of the units are presented correctly.

**Answer:** it is correct

Q4

**Query:** Have all of the funders of your work been fully and accurately acknowledged? If not, please ensure you make appropriate changes to the Acknowledgements text

**Answer:** yes

Q5

**Query:** Ref. 1: Please provide the page (or article) number(s).

**Answer:** I provided the page number on the proof

Q6

**Query:** Ref. 17: Please provide the page (or article) number(s).

**Answer:** I provided the page number on the proof

Q7

**Query:** Ref. 19: Can this reference be updated? Please supply details to allow readers to access the reference (for references where page numbers are not yet known, please supply the DOI).

**Answer:**

page 106740

[doi.org/10.1016/j.mssp.2022.106740](https://doi.org/10.1016/j.mssp.2022.106740)

**Query:** Ref. 35: Please provide the page (or article) number(s).

**Answer:** page 203105 1-9